processes

MDPI

Article

Sustainable Production of 2,5-Furandicarboxylic Acid via Nickel-Based Heterogeneous Catalysis from 5-Hydroxymethylfurfural

Celso Luiz de Aquino Santos [1], João Paulo Alves Silva [1], Solange I. Mussatto [2,*] and Livia Melo Carneiro [1]

[1] Department of Chemical Engineering, Engineering School of Lorena, University of São Paulo, Lorena 12.602-810, SP, Brazil; celsoluiz@usp.br (C.L.d.A.S.); jpalves80@usp.br (J.P.A.S.); liviacarneiro@usp.br (L.M.C.)
[2] Department of Biotechnology and Biomedicine, Technical University of Denmark, Søltofts Plads, Building 223, 2800 Kongens Lyngby, Denmark
* Correspondence: smussatto@dtu.dk or solangemussatto@hotmail.com

Abstract

2,5-Furandicarboxylic acid (FDCA) is a bio-based platform chemical with high potential to replace terephthalic acid in polymer production, particularly for polyethylene furanoate (PEF), a biopolymer with superior thermal and barrier properties. This study investigates the selective oxidation of 5-hydroxymethylfurfural (HMF) into FDCA using nickel-based heterogeneous catalysts, aiming at a cost-effective and sustainable alternative to noble metal catalysts. A series of nickel oxide catalysts were synthesized and screened. The NiOx catalyst synthesized without thermal treatment via Route B showed the best performance, achieving a FDCA yield of 11.77%, selectivity of 27.41%, and concentration of 0.9 g/L under preliminary conditions. Reaction kinetics revealed that the controlled addition of NaClO enhanced FDCA yield by 2.28 times. Optimization using a 2^3 factorial design identified the optimal conditions as 6% (w/v) catalyst concentration, 25 °C, and a NaClO:HMF molar ratio of 12:1, leading to 34.14% yield and 42.57% selectivity. The NiOx catalyst maintained its activity over five successive cycles, indicating good recyclability. Moreover, NiOx demonstrated catalytic activity with crude HMF derived from glucose dehydration, confirming its practical applicability. These results support the potential of nickel-based catalysts in sustainable FDCA production, contributing to the advancement of bio-based polymer synthesis.

Keywords: 2,5-furandicarboxylic acid; 5-hydroxymethylfurfural; heterogeneous catalyst; Nickel oxide; bio-based polymers

check for updates

Received: 15 May 2025
Revised: 19 June 2025
Accepted: 24 June 2025
Published: 26 June 2025

Citation: de Aquino Santos, C.L.; Silva, J.P.A.; Mussatto, S.I.; Carneiro, L.M. Sustainable Production of 2,5-Furandicarboxylic Acid via Nickel-Based Heterogeneous Catalysis from 5-Hydroxymethylfurfural. *Processes* **2025**, *13*, 2026. https://doi.org/10.3390/pr13072026

Copyright: © 2025 by the authors. Licensee MDPI, Basel, Switzerland. This article is an open access article distributed under the terms and conditions of the Creative Commons Attribution (CC BY) license (https://creativecommons.org/licenses/by/4.0/).

1. Introduction

The growing concern over climate change and the environmental impact of fossil-based resources has intensified the search for renewable alternatives in chemical production. Among these, biomass-derived platform molecules have garnered increasing attention due to their potential to replace petroleum-based feedstocks in a variety of chemical processes, thereby contributing to the development of a sustainable and circular bioeconomy [1].

In this context, 2,5-furandicarboxylic acid (FDCA) has emerged as a promising bio-based monomer, particularly to produce polyethylene furanoate (PEF), an alternative to polyethylene terephthalate (PET), the most widely used fossil-based polymer in the packaging industry [2–5].

FDCA can be obtained from 5-hydroxymethylfurfural (HMF), a versatile intermediate derived from the acid-catalyzed dehydration of hexoses such as glucose and fructose (Figure 1) [6]. HMF is considered one of the most important biomass-derived platform chemicals due to its potential to be converted into a wide range of value-added compounds, including biofuels, pharmaceuticals, solvents, and monomers for biopolymers. Among the derivatives of HMF, FDCA has attracted considerable interest because of its structural similarity to terephthalic acid (TPA) and its superior properties in polymer applications [2].

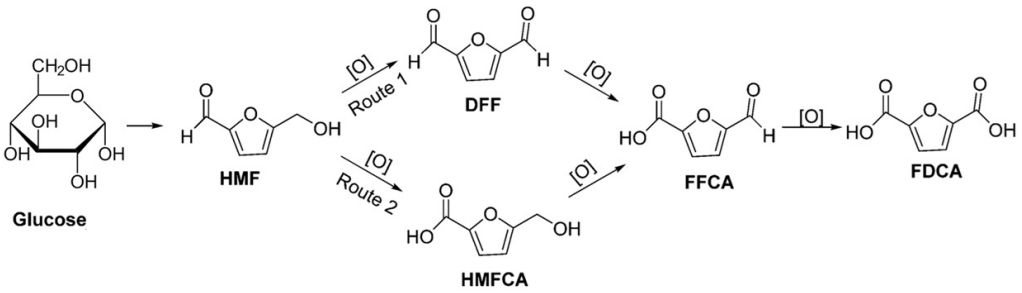


Figure 1. Schematic pathways for the conversion of glucose to 5-hydroxymethylfurfural (HMF) via dehydration and for the subsequent oxidation of HMF to 2,5-furandicarboxylic acid (FDCA). HMF is oxidized either via Route 1 through 2,5-diformylfuran (DFF) or via Route 2 through 5-hydroxymethyl-2-furancarboxylic acid (HMFCA), with both routes converging at 5-formyl-2-furancarboxylic acid (FFCA) before the final oxidation to FDCA. [O] denotes the oxidant. Adapted from Tamboli et al. [7].

Despite its potential, the commercial production of FDCA remains limited, mainly due to challenges associated with the catalytic oxidation of HMF. The most efficient processes reported to date rely on noble metal catalysts such as Au, Pt, Pd, and Ru [4], typically supported on metal oxides or carbon-based materials [8]. These systems often require alkaline reaction media (e.g., NaOH), which not only increase operational costs but also promote undesired side reactions, HMF degradation, and the formation of large quantities of saline waste upon neutralization [1]. Moreover, the high cost and limited availability of noble metals hinder the scalability and economic viability of such processes [3].

Nickel-based catalysts have emerged as attractive candidates for HMF oxidation due to their low cost, environmental compatibility, and promising catalytic performance [9–11]. Nickel oxides have demonstrated the ability to selectively oxidize HMF into FDCA in the presence of various oxidants, including molecular oxygen, hydrogen peroxide, and sodium hypochlorite (NaClO) [12,13]. Additionally, nickel catalysts often exhibit good thermal and chemical stability, making them suitable for repeated use in both batch and continuous processes [14,15].

This study aims to contribute to the advancement of nickel-based catalytic systems for the sustainable production of FDCA from HMF. The main objective is to evaluate the selective oxidation of HMF into FDCA using nickel oxide (NiOx) catalysts synthesized via different routes, under mild reaction conditions and employing NaClO as the oxidant. A key focus of this study is to identify the optimal catalyst preparation method and reaction conditions that maximize FDCA yield and selectivity, while maintaining high catalyst stability and recyclability.

Kinetic experiments were conducted to investigate the influence of oxidant dosing strategy and reaction time on FDCA production. A 2^3 statistical factorial design was then applied to optimize catalyst concentration, reaction temperature, and NaClO:HMF molar ratio. Catalyst recyclability was also evaluated under optimized conditions. Finally, the performance of the NiOx catalyst was assessed using crude HMF obtained from glucose dehydration, highlighting the practical applicability of the system to real biomass feedstocks [16].

The findings of this study provide new insights into the development of sustainable and cost-effective catalytic routes for FDCA production, demonstrating that non-noble metal catalysts such as NiOx can deliver promising results under mild and environmentally friendly conditions.

2. Materials and Methods

2.1. Materials and Reagents

All reagents were of analytical grade and were used as received, without further purification. 5-Hydroxymethylfurfural (HMF, ≥98% purity) was purchased from Merck Brazil (Sigma-Aldrich). Nickel(II) sulfate hexahydrate ($NiSO_4 \cdot 6H_2O$, ≥98.5%) and sodium hydroxide (NaOH, ≥97%) were obtained from Synth. Sodium hypochlorite (NaClO) solution was freshly prepared from a commercial stock (12% w/v, ACS reagent grade) and standardized prior to use. D-(+)-Glucose (≥99.5%) was used to produce crude HMF and was acquired from Merck. $NbOPO_4$ was obtained from CBMM (Companhia Brasileira de Metalurgia e Mineração). Deionized water (resistivity ≥ 18.2 MΩ·cm) was used throughout all experiments, including catalyst synthesis, reaction media, and sample dilution for analytical purposes.

2.2. Synthesis of Nickel-Based Catalysts

Nickel-based catalysts were synthesized using two distinct precipitation routes, referred to as Route A and Route B, as shown schematically in Figure 2. These approaches aimed to evaluate the influence of synthesis conditions on the physicochemical properties and catalytic performance of the resulting materials.

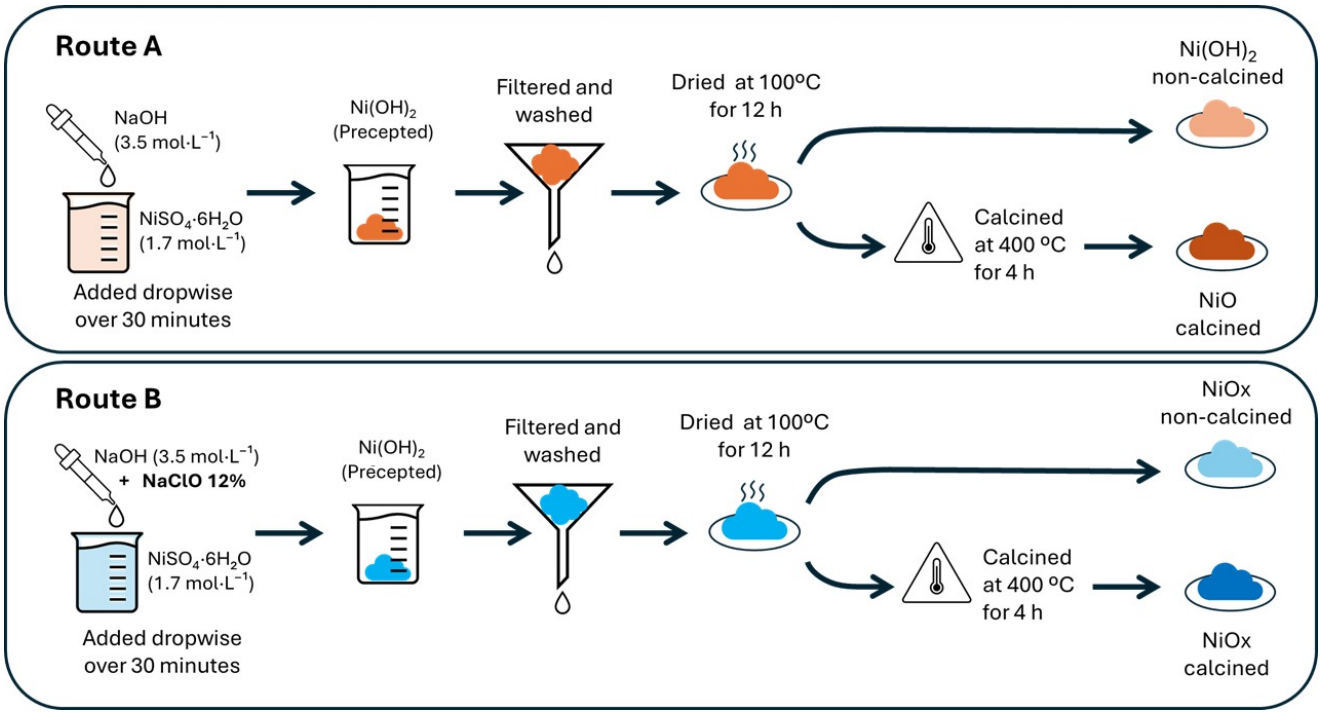


Figure 2. Schematic representation of the synthesis of nickel-based catalysts via two precipitation routes. In (**Route A**), a 3.5 mol·L^{-1} NaOH solution was added dropwise (30 min) to 1.7 mol·L^{-1} $NiSO_4 \cdot 6H_2O$, the precipitate was filtered, washed to neutral pH, and dried at 100 °C (12 h) to yield $Ni(OH)_2$; optional calcination at 400 °C (4 h, 5 °C·min^{-1} ramp, static air) afforded NiOcalc. In (**Route B**), NaOH (3.5 mol·L^{-1} in 12% NaClO) was added under identical conditions to $NiSO_4 \cdot 6H_2O$ to produce a slurry that, after filtration, washing, and drying, yielded NiOx; subsequent calcination under the same thermal protocol produced NiOx-calc. This design allows the evaluation of synthesis-condition effects on catalyst structure and performance.

Route A: In this method, 100 mL of 3.5 mol·L^{-1} solution of NaOH was added dropwise over 30 min using a peristaltic pump to control the precipitation rate into a 1.7 mol·L^{-1} $NiSO_4 \cdot 6H_2O$ solution. The resulting precipitate was filtered, washed with deionized water until neutral pH, and dried at 100 °C for 12 h. Samples obtained from Route A were designated as $Ni(OH)_2$ (non-calcined) and NiOcalc (calcined at 400 °C for 4 h in static air).

Route B: In this alternative approach, 100 mL of 3.5 mol·L^{-1} solution of NaOH prepared in 100 mL of aqueous solution of NaClO 12% was added dropwise over 30 min using a peristaltic pump to control the precipitation rate to a 1.7 mol·L^{-1} $NiSO_4 \cdot 6H_2O$ solution. The resulting slurry was filtered, washed, and dried under the same conditions as in Route A. The non-calcined material was named NiOx. An additional sample, NiOx-calc, was obtained by calcining the precursor at 400 °C for 4 h.

The calcination step was performed in a muffle furnace with a heating ramp of 5 °C·min^{-1} under static air to investigate the effect of thermal treatment on crystallinity, surface area, and catalytic behavior.

2.3. Catalyst Characterization

The catalysts were characterized to determine their structural, textural, thermal, and morphological properties.

X-ray Diffraction (XRD): Measurements were performed a MiniFlex 600 diffractometer (Rigaku Corporation, Japan), with CuKα radiation (λ = 1.5418 Å). Patterns were collected from 10° to 90° (2θ), with a step size of 0.02° and scan speed of 1°·min^{-1}. The average crystallite size of the calcined samples was estimated using the Scherrer equation, based on the (2 0 0) reflection at $2\theta \approx 43.3°$. A shape factor of 0.9 and Cu Kα radiation (λ = 1.5418 Å) were used. FWHM values were obtained after baseline correction.

Fourier-Transform Infrared Spectroscopy (FTIR): Spectra were recorded using a Perkin Elmer Frontier FTIR spectrometer equipped with an attenuated total reflectance (ATR) module. Spectra were recorded from 4000 to 450 cm^{-1} with a resolution of 4 cm^{-1} and 64 scans.

Thermogravimetric Analysis (TGA): Conducted with a Netzsch STA 443 Jupiter analyzer (Netzsch-Gerätebau, Germany). Approximately 10 mg of sample was heated from 30 °C to 1000 °C at 10 °C·min^{-1} under nitrogen flow (100 mL·min^{-1}).

Scanning Electron Microscopy with Energy-Dispersive X-ray Spectroscopy (SEM-EDX): Images were captured using a Tescan Mira microscope at 10 kV (Tescan Orsay Holding, Czech Republic). Samples were mounted on aluminum stubs and coated with a thin gold layer prior to analysis. Energy-dispersive X-ray (EDX) spectroscopy was employed for semi-quantitative elemental mapping.

Nitrogen Physisorption (BET Analysis): Surface area, pore volume, and pore diameter were determined from N_2 adsorption–desorption isotherms at −196 °C using a QuantaChrome Nova 2200e analyzer (USA, QuantaChrome Instruments). Prior to measurement, samples were degassed at 200 °C under vacuum for 2 h. Surface area was calculated by the Brunauer–Emmett–Teller (BET) method, and pore size distribution was estimated using the Barrett–Joyner–Halenda (BJH) model.

2.4. Catalytic Oxidation of HMF to FDCA

The catalytic performance of the prepared materials was evaluated in batch mode under atmospheric pressure in an aqueous medium in the absence of added base (i.e., alkalinity solely derived from ClO^- hydrolysis). Experiments were conducted in 100 mL glass-jacketed reactors with magnetic stirring (600 rpm). The reaction temperature was controlled using a thermostatic water bath with precision of ±0.5 °C.

In a typical run, 50 mL of an aqueous solution containing 60 mmol·L^{-1} HMF and a defined concentration of catalyst (2–6% w/v) was prepared. Sodium hypochlorite was added either in a single batch or gradually (dropwise over 30 min), maintaining molar ratios of NaClO:HMF between 6:1 and 12:1. Reaction temperature ranged from 25 °C to 75 °C depending on the experimental design.

At defined time intervals, 0.5 mL aliquots were withdrawn, filtered through 0.22 µm nylon membranes, and immediately diluted for HPLC analysis.

2.5. Kinetic Studies

Kinetic assays were carried out under both standard and optimized conditions to investigate the influence of reaction time, and the mode of oxidizing agent addition. The reaction kinetics were monitored for 60 min. Reactions were performed using 2% (w/v) catalyst at 25 °C, a NaClO:HMF molar ratio of 6:1, and 50 mL of a 60 mmol·L^{-1} HMF solution. Samples were collected at t = 0, 10, 20, 30, 40, 50, and 60 min and analyzed by HPLC. Table 1 summarizes the various NaClO addition strategies tested in the experiments.

Table 1. Evaluation of the reaction kinetics for FDCA production.

Assay	Oxidant (NaClO) Addition Method
C1	100% of the volume added at t = 0 min
C2	50% of the volume added at t = 0 min and 50% at t = 30 min
C3	25% of the volume added at each of t = 0, 10, 20, and 30 min
C4	100% of the volume added continuously from t = 0 min to t = 30 min at a constant flow rate using a peristaltic pump

2.6. Experimental Design for FDCA Production

A 2^3 full factorial design was employed to identify the most influential parameters affecting FDCA yield and selectivity. The variables investigated were as follows: (A) catalyst concentration (2, 4, and 6% w/v); (B) reaction temperature (25, 50, and 75 °C); (C) NaClO:HMF molar ratio (6:1, 9:1, 12:1). The central point (4% w/v, 50°C, 9:1) was evaluated in triplicate to estimate experimental error. FDCA yield, HMF conversion, selectivity, and productivity were considered as response variables. Data were analyzed using analysis of variance (ANOVA) and response surface methodology (RSM), and model adequacy was verified through the coefficient of determination (R^2) and residual analysis.

2.7. Catalyst Recycling Tests

To evaluate catalyst's stability, the NiOx catalyst was reused in five consecutive oxidation cycles under optimal reaction conditions. After each cycle, the catalyst was recovered by vacuum filtration, washed thoroughly with deionized water, and dried at 60 °C for 12 h prior to reuse. Catalytic activity and selectivity were monitored throughout the cycles, and the recovered materials were characterized by XRD and SEM to assess morphological and structural stability.

2.8. Oxidation of Crude HMF

Crude HMF was obtained by dehydrating glucose using water as the solvent and $NbOPO_4$ as the catalyst. The reaction was carried out at 160 °C for 30 min in a sealed flask with magnetic stirring. The concentration of HMF was determined by HPLC. The resulting solution, containing approximately 8.4 g·L^{-1} of HMF, was directly used in the oxidation reaction under optimized conditions for FDCA production.

2.9. Analytical Methods

Quantification of HMF and FDCA was performed by high-performance liquid chromatography (HPLC) using a Waters Alliance 2695 system equipped with a refractive index detector (RID) and a UV detector set at 263 nm. The column used was Aminex HPX-87H (300 × 7.8 mm) operated at 45 °C. The mobile phase consisted of 0.005 mol·L^{-1} H_2SO_4 at a flow rate of 0.6 mL·min^{-1}. External calibration curves ($R^2 > 0.999$) were prepared using standard solutions ranging from 0.1 to 10.0 g·L^{-1}.

3. Results and Discussion

3.1. Catalyst Characterization

The physicochemical characterization of the nickel-based catalysts revealed strong correlations between the preparation route, thermal treatment, and catalytic performance. X-ray diffraction (XRD) patterns (Figure 3) confirmed that NiOx prepared via Route B without calcination exhibited a predominantly amorphous structure, with poorly defined crystalline peaks. In contrast, thermally treated catalysts (NiOx-calc and NiOcalc) displayed intense reflections at 2θ ≈ 37.2°, 43.3°, and 62.9°, consistent with the cubic NiO phase, in agreement with previous studies [9,17–19]. The crystallite size was estimated to be 12 nm for NiOx-calc and 6 nm for NiOcalc, using the Scherrer equation at the 43.3° peak.

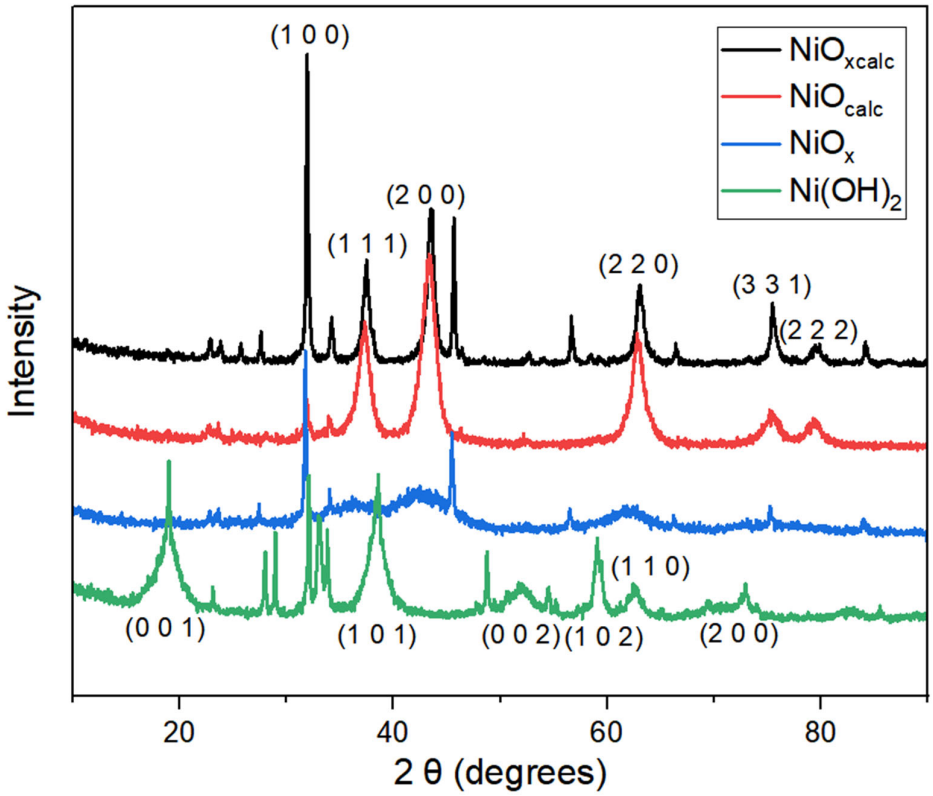


Figure 3. X-ray diffractograms of the catalysts produced.

The comparative XRD patterns of $Ni(OH)_2$, NiOx, NiOcalc, and NiOx-calc (Figure 3) further illustrate the evolution of crystallinity and phase composition upon calcination. The green pattern, corresponding to $Ni(OH)_2$, shows broad peaks around 2θ = 19.2°, 33.1°, and 38.5°, which are consistent with the layered structure of nickel hydroxide The crystallite size was estimated to be 7 nm for $Ni(OH)_2$, using the Scherrer equation at the 38.5°peak [20].

The blue pattern (NiOx) displays a largely amorphous profile with only very weak reflections, indicating poor long-range order. The crystallite size was estimated to be greater than 100 nm for NiOx, using the Scherrer equation at the 43.3°peak. Upon calcination, both

NiOcalc (red) and NiOx-calc (black) exhibit sharp and intense diffraction peaks, particularly at 2θ ≈ 37.2°, 43.3°, and 62.9°, characteristic of the (1 1 1), (2 0 0), and (2 2 0) planes of crystalline NiO, matching JCPDS card no. 47-1049. This confirms the thermal transformation of nickel hydroxide and peroxo-oxides into the well-crystallized NiO phase [21].

The FTIR spectra (Figure 4) confirmed the presence of vibrational modes characteristic of Ni–O at 517 cm^{-1} and Ni–OH stretching at 3640 cm^{-1}. These surface hydroxyls are considered catalytically relevant, particularly in oxidation reactions involving oxygenated species such as HMF [14,22,23]. In addition, a broad O–H stretching band at 3415 cm^{-1} and H–O–H bending vibration at 1620 cm^{-1} indicate the presence of adsorbed water layers. A secondary Ni–O band at 568 cm^{-1} is associated with disordered or hydroxylated sites, while an additional feature at 620 cm^{-1} suggests defect-related amorphous NiOx phases [19].

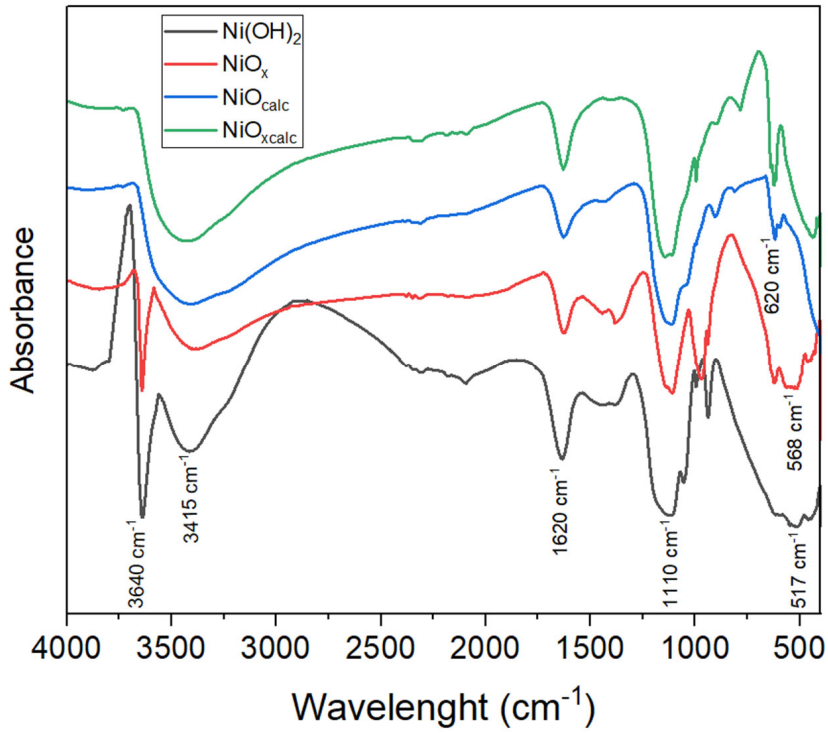


Figure 4. FTIR spectra of the catalysts $Ni(OH)_2$, NiOx, NiOcalc, and NiOx-calc.

Scanning electron microscopy (Figure 5) revealed clear morphological differences among the samples. While NiOcalc and NiOx-calc exhibited highly aggregated crystalline domains, NiOx displayed an amorphous, porous, and irregular structure with micro-agglomerates, which may favor the dispersion of active sites. This morphology likely contributes to the superior performance of NiOx in oxidation reactions [9,17,18].

Thermogravimetric analysis (Figure 6) indicated three major weight-loss stages. The second event (M_2), occurring at approximately 240 °C, can be attributed to the decomposition of NiOx into NiO, corroborating the presence of labile oxygen species [24–26]. The total mass loss was approximately 23%, in agreement with the literature values for nickel hydroxide or peroxo-oxide systems.

Textural analysis by nitrogen adsorption (Table 2) revealed a surface area of 59.1 $m^2\ g^{-1}$, a pore volume of 0.1 cm^3/g, and an average pore diameter of 6.7 nm. These values are lower than those reported by Liu et al. [9] and Lai et al. [25] for NiOx (202 m^2/g), yet still sufficient for mesoporous catalytic behavior. The relatively larger pore diameter observed here may facilitate diffusion of bulkier intermediates such as HMFCA and FFCA, although at the cost of lower specific surface area.

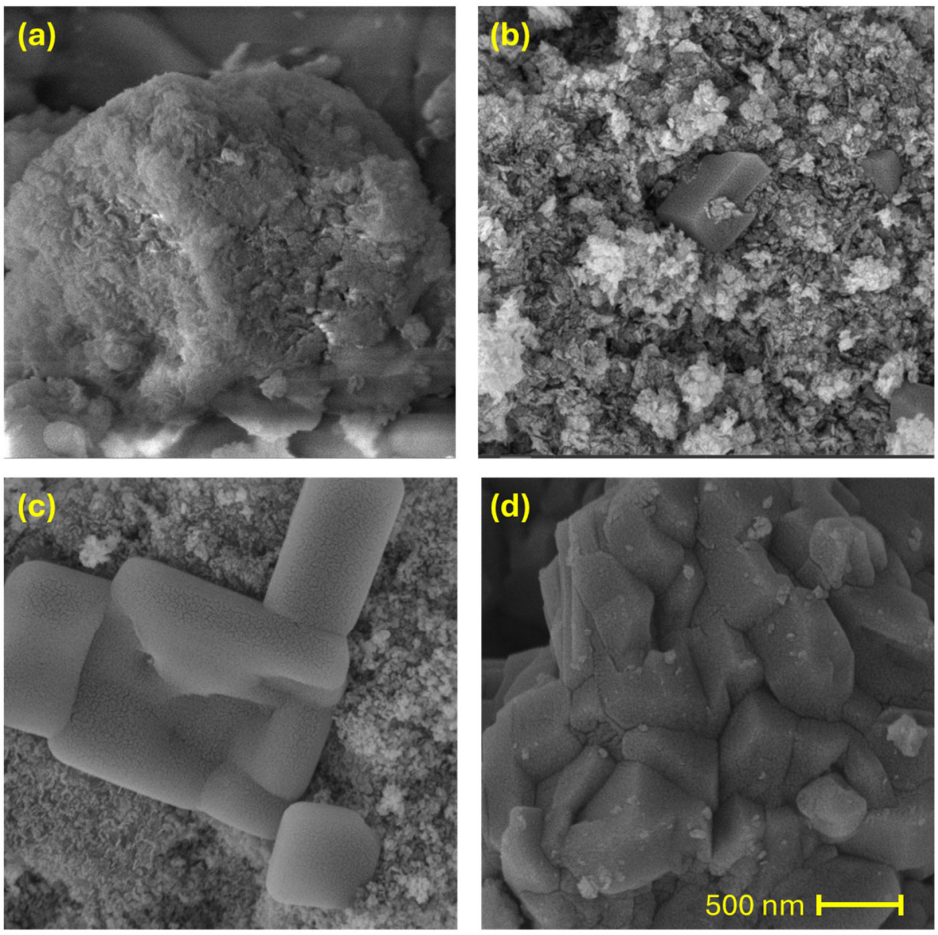


Figure 5. Micrographs of catalysts: (**a**) $Ni(OH)_2$, (**b**) NiOcalc, (**c**) NiOx-calc, and (**d**) NiOx, all taken at 100,000× magnification with a 500 nm scale bar.

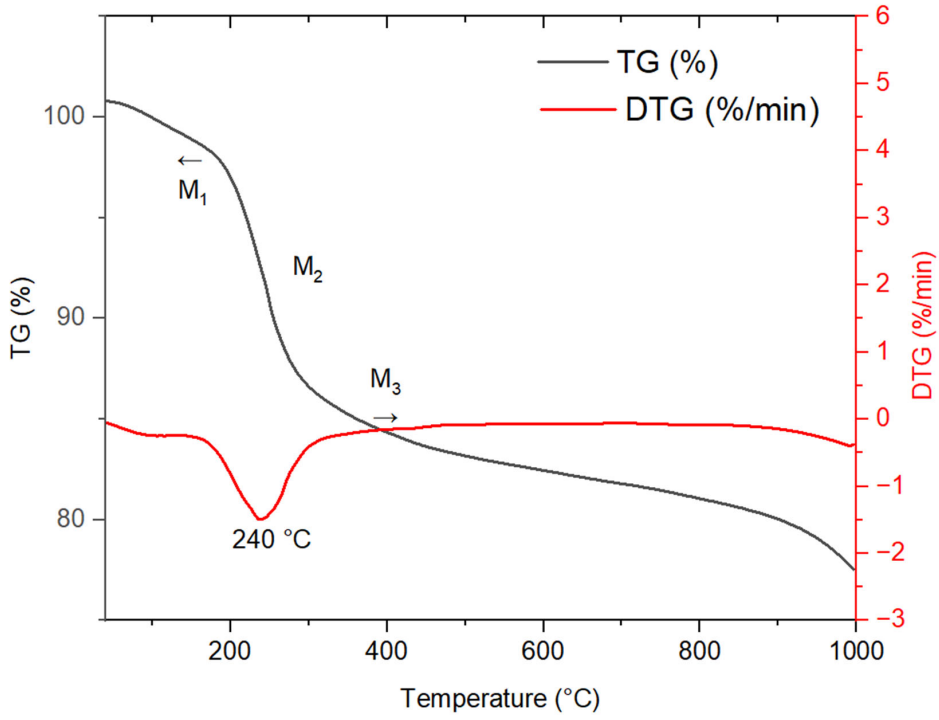


Figure 6. Thermogravimetric (TG) analysis of NiOx.

Table 2. Surface area, pore volume, and pore diameter of the best-performing catalyst.

Catalyst	Surface Area (m^2 g^{-1})	Total Pore Volume (cm^3 g^{-1})	Average Pore Diameter (nm)
NiOx	59.1	0.1	6.7

Taken together, these findings support the conclusion that the NiOx catalyst exhibits a combination of structural disorder, accessible surface area, and active oxygenated species—features that contribute directly to its catalytic efficiency in FDCA production.

3.2. Influence of Synthesis Route and Calcination Conditions on Catalyst Properties

The influence of catalyst synthesis parameters was assessed using a 2^2 factorial design, with synthesis route (A or B) and calcination (with or without) as independent variables. The response variables were FDCA concentration, yield, selectivity, and HMF conversion (Table 3). Among the four catalysts evaluated, NiOx (Route B, no calcination) showed the best overall performance, with 0.90 $g.L^{-1}$ FDCA, 11.77% yield, 27.41% selectivity, and 42.93% conversion, consistent with results reported by Liu et al. [9].

Table 3. A 2^2 factorial design to evaluate the effects of synthesis route and calcination of nickel heterogeneous catalysts.

Catalyst	Route	Calcination (400 °C; 4 h)	FDCA Concentration (g/L)	FDCA Yield (%)	FDCA Selectivity (%)	HMF Conversion (%)
$Ni(OH)_2$	A	NO	0.01	0.13	0.28	47.15
			0.01	0.13	0.26	50.41
NiOcalc	A	YES	0.17	2.22	5.82	38.21
			0.13	1.96	4.82	40.65
NiOx	B	NO	0.90	11.77	27.41	42.93
			0.89	11.64	26.02	44.72
NiOx-calc	B	YES	0.21	2.75	6.65	41.30
			0.23	3.01	6.75	44.55

In contrast, the $Ni(OH)_2$ precursor and the thermally treated NiOx-calc and NiOcalc exhibited significantly lower catalytic activity (e.g., $Ni(OH)_2$ showed <1% yield). This difference in the performance of the prepared catalysts was somehow expected, as changes in synthesis routes and thermal treatment methods can significantly alter the composition and structure of non-stoichiometric nickel oxide, leading to variations in key characteristics such as nickel oxidation state, the presence of active oxygen species, and catalyst morphology [23].

Statistical analysis of the ANOVA results (Tables 4–7) confirmed that both synthesis route and calcination had statistically significant effects ($p < 0.01$) on all response variables. For FDCA concentration (Table 4), the synthesis route accounted for more than 48% of the variance, while calcination explained an additional 15%. The interaction between the two factors also showed a strong effect, with a model fit ($R^2 = 0.99887$).

This interaction is illustrated in Figure 7, which shows that Route B without calcination outperformed all other combinations in terms of FDCA concentration, yield, and selectivity. Only in the case of HMF conversion did the interaction slightly favor thermally treated catalysts from Route B (Figure 7d), suggesting that crystallinity may enhance substrate activation but not necessarily product selectivity.

Table 4. Analysis of variance (ANOVA) for the 2^2 factorial design: main effects and factor interactions on FDCA concentration (g L^{-1}).

C_{FDCA}	Sum of Squares	Degrees of Freedom	Mean Squares	F Value	*p*-Value
Route (1)	0.456013	1	0.456013	1737.190	0.000002 *
Calcination (2)	0.143113	1	0.143113	545.190	0.000020 *
1 × 2	0.332113	1	0.332113	1265.190	0.000004 *
Error	0.001050	4	0.000263		
Total SS	0.932287	7			R^2 = 0.99887

* Significant at the 99% confidence level ($p < 0.01$).

Table 5. Analysis of variance (ANOVA) for the 2^2 factorial design: main effects and factor interactions on FDCA yield (%).

Y_{FDCA}	Sum of Squares	Degrees of Freedom	Mean Squares	F Value	*p*-Value
Route (1)	76.4466	1	76.44661	4020.861	0.000000 *
Calcination (2)	23.5641	1	23.56411	1239.401	0.000004 *
1 × 2	58.1581	1	58.15811	3058.941	0.000001 *
Error	0.0760	4	0.01901		
Total SS	158.2449	7			R^2 = 0.99952

* Significant at the 99% confidence level ($p < 0.01$).

Table 6. Analysis of variance (ANOVA) for the 2^2 factorial design: main effects and factor interactions on FDCA selectivity (%).

S_{FDCA}	Sum of Squares	Degrees of Freedom	Mean Squares	F Value	*p*-Value
Route (1)	387.1153	1	387.1153	1052.480	0.000005 *
Calcination (2)	111.9756	1	111.9756	304.437	0.000063 *
1 × 2	314.1271	1	314.1271	854.041	0.000008 *
Error	1.4713	4	0.3678		
Total SS	814.6893	7			R^2 = 0.99819

* Significant at the 99% confidence level ($p < 0.01$).

Table 7. Analysis of variance (ANOVA) for the 2^2 factorial design: main effects and factor interactions on HMF conversion (%).

X_{HMF}	Sum of Squares	Degrees of Freedom	Mean Squares	F Value	*p*-Value
Route (1)	1.0658	1	1.06580	0.28096	0.624133
Calcination (2)	52.5313	1	52.53125	13.84779	0.020452 *
1 × 2	35.70125	1	35.70125	9.41123	0.037374 *
Error	15.1739	4	3.79347		
Total SS	104.4722	7			R^2 = 0.85476

* Significant at the 99% confidence level ($p < 0.01$).

These findings align with reports from Holzhäuser et al. [15] and Herlina et al. [14], who observed that amorphous or partially hydroxylated Ni-based catalysts outperformed fully crystalline NiO in base-free HMF oxidation. This enhanced performance is likely due to greater availability of surface hydroxyl groups and the flexibility of redox-active Ni(II)/Ni(III) centers.

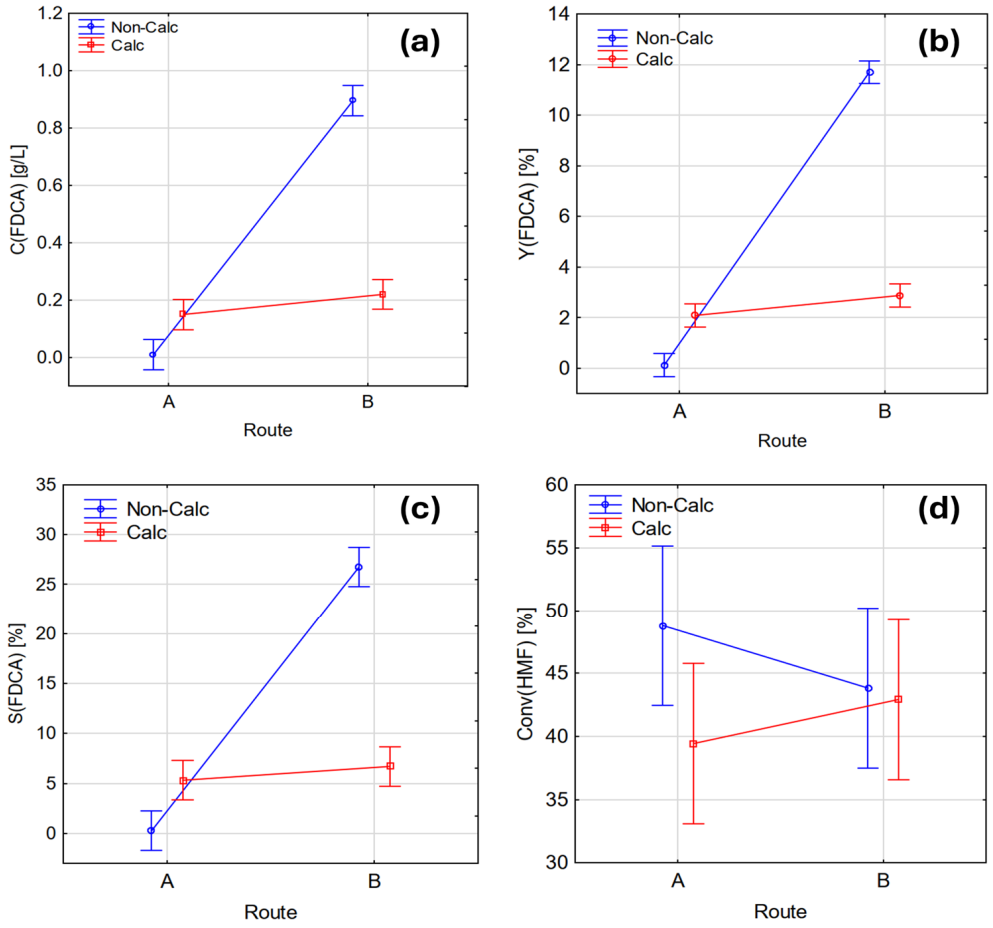


Figure 7. Interaction effect of the independent variables synthesis route and calcination on (**a**) FDCA concentration, (**b**) FDCA yield, (**c**) FDCA selectivity, and (**d**) HMF conversion in the 2^2 factorial design.

3.3. Reaction Kinetics and Oxidant Addition Strategies

The catalytic oxidation of HMF to FDCA was evaluated under batch conditions, using NiOx as the catalyst, under four different oxidant-addition modes. The time-course data presented in Figure 8 demonstrates that HMF conversion reaches a plateau as soon as the oxidant feed is completed, indicating a direct correlation between HMF conversion and the amount of oxidant present in the medium. Consequently, HMF conversion (Figure 8b) clearly depends on the temporal availability of NaClO in the reaction mixture.

In contrast, FDCA formation continues up to t = 50 min (Figure 8a). This behavior is consistent with the mechanism proposed in the literature [8,9,27], in which HMF is first oxidized to the intermediate HMFCA, which is sequentially converted to FFCA and finally to FDCA. It is therefore expected to observe HMF depletion first, followed by a gradual increase in FDCA concentration. The maximum FDCA yield was 13.7%, with HMF conversion of 43.5%.

One of the most relevant findings from the kinetic study was the significant impact of the oxidant addition mode. When NaClO was added all at once at the beginning of the reaction, FDCA yield was notably lower, and the formation of degradation products increased. In contrast, controlled addition of NaClO over 30 min led to a 2.28-fold increase in FDCA yield (Figure 8), reaching 13.7% compared to 6.0% under otherwise identical conditions. This improvement is attributed to a more stable pH profile and the minimization of side reactions, such as HMF ring opening and chlorination [4,28,29].

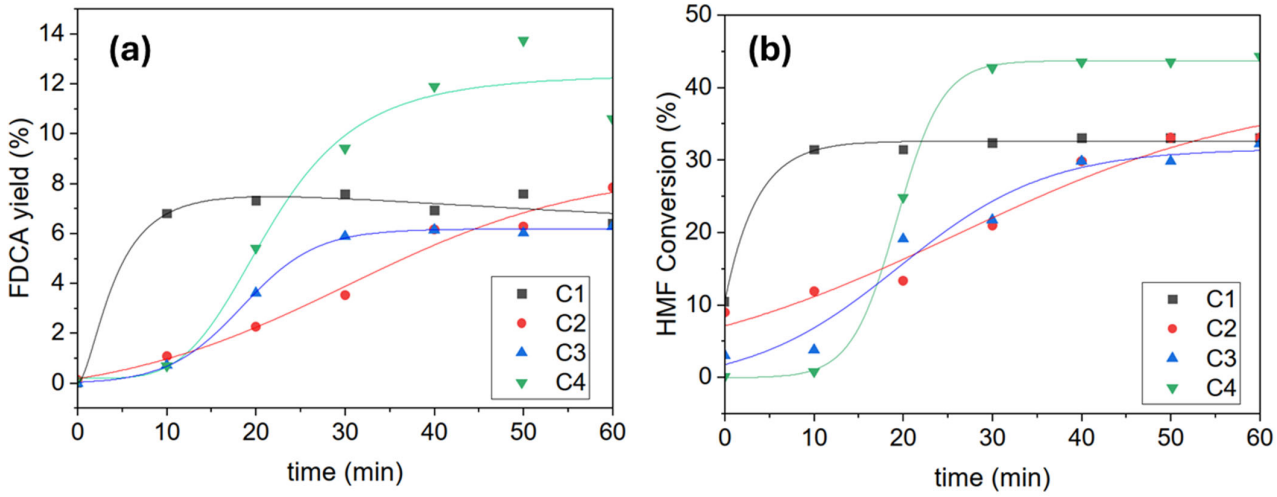


Figure 8. Kinetics of FDCA production from pure HMF using the NiOx catalyst: (**a**) FDCA yield; (**b**) HMF conversion. C1: 100% of the volume added at t = 0 min; C2: 50% of the volume added at t = 0 and 30 min; C3: 25% of the volume added at t = 0, 10, 20, and 30 min; C4: 100% of the volume added continuously from t = 0 to t = 30 min at a constant flow rate using a peristaltic pump.

The positive influence of gradual oxidant addition corroborates previous findings by Luo et al. [13], who demonstrated that slow oxidant dosing extends catalyst lifetime and suppresses overoxidation. These results underscore the importance of temporal control over oxidant availability to promote the desired oxidation pathway while minimizing non-selective degradation.

3.4. Reaction Optimization Using Factorial Design

To further optimize the reaction parameters, a 2^3 full factorial design was employed with the following factors: (A) catalyst concentration (2–6% *w*/*v*); (B) beaction temperature (25–75 °C); and (C) NaClO:HMF molar ratio (6:1–12:1). The response variables analyzed were FDCA concentration, yield, and selectivity, and HMF conversion (Table 8). The analysis of variance (ANOVA) revealed that catalyst concentration and oxidant ratio were the most significant factors across all responses ($p < 0.01$), while temperature showed only a marginal effect ($p > 0.05$).

Pareto charts for FDCA concentration (Figure 9a) and yield (Figure 9b) confirm the dominant role of catalyst loading and oxidant excess in improving performance. The NaClO:HMF molar ratio exhibited a strong linear and quadratic influence, suggesting that an adequate oxidant supply is critical for driving the multistep oxidation sequence toward FDCA. However, excessive oxidant may reduce selectivity due to competing degradation pathways.

The response surface plot for FDCA yield (Figure 10b) reveals that the optimal region lies at 6% catalyst loading, 25 °C, and 12:1 molar ratio, conditions under which a maximum FDCA yield of 34.14% and selectivity of 42.57% were achieved (Table 8). Under these conditions, HMF conversion reached 80.2% with minimal accumulation of intermediates. Similar trends were observed for concentration (Figure 10a) and selectivity (Figure 10c), both of which improved significantly at moderate catalyst loadings and oxidant ratios.

Notably, operating at 25 °C was sufficient to ensure high conversion (Figure 10d), reinforcing the advantage of NiOx in low-temperature oxidation systems compared to noble-metal catalysts that typically require elevated temperatures and pressurized O_2 [12,15].

Table 8. Results of the 2^3 factorial design, performed in duplicate, with a triplicate at the center point, for identifying the variables with the greatest influence on the oxidation of HMF to FDCA.

Assay	Experimental Conditions			Response Variables			
	Catalyst% (*w*/*v*)	Temperature (°C)	NaClO: HMF	[FDCA] (g L^{-1})	FDCA Yield (%)	FDCA Selectivity (%)	HMF Conversion (%)
1	2	25	6:1	1.10	14.38	25.94	55.45
				1.02	13.34	24.19	55.12
2	6	25	6:1	1.21	15.82	27.10	58.37
				1.17	15.30	26.73	57.24
3	2	75	6:1	0.66	8.63	15.52	55.61
				0.80	10.46	23.48	44.55
4	6	75	6:1	1.06	13.86	18.73	73.98
				1.03	13.47	17.97	74.96
5	2	25	12:1	1.79	26.92	34.30	78.49
				1.93	29.03	36.89	78.68
6	6	25	12:1	2.27	34.14	42.57	80.19
				2.03	30.53	37.11	82.26
7	2	75	12:1	1.02	15.34	22.46	68.30
				1.09	16.39	24.75	66.23
8	6	75	12:1	1.81	27.22	32.49	83.77
				1.61	24.21	28.97	83.58
9	4	50	9:1	1.36	18.98	26.97	70.38
				1.50	20.94	31.13	67.25
10	4	50	9:1	1.38	19.26	29.10	66.20
				1.47	20.52	32.09	63.94
11	4	50	9:1	1.42	19.82	28.66	69.16
				1.55	21.63	32.59	66.38

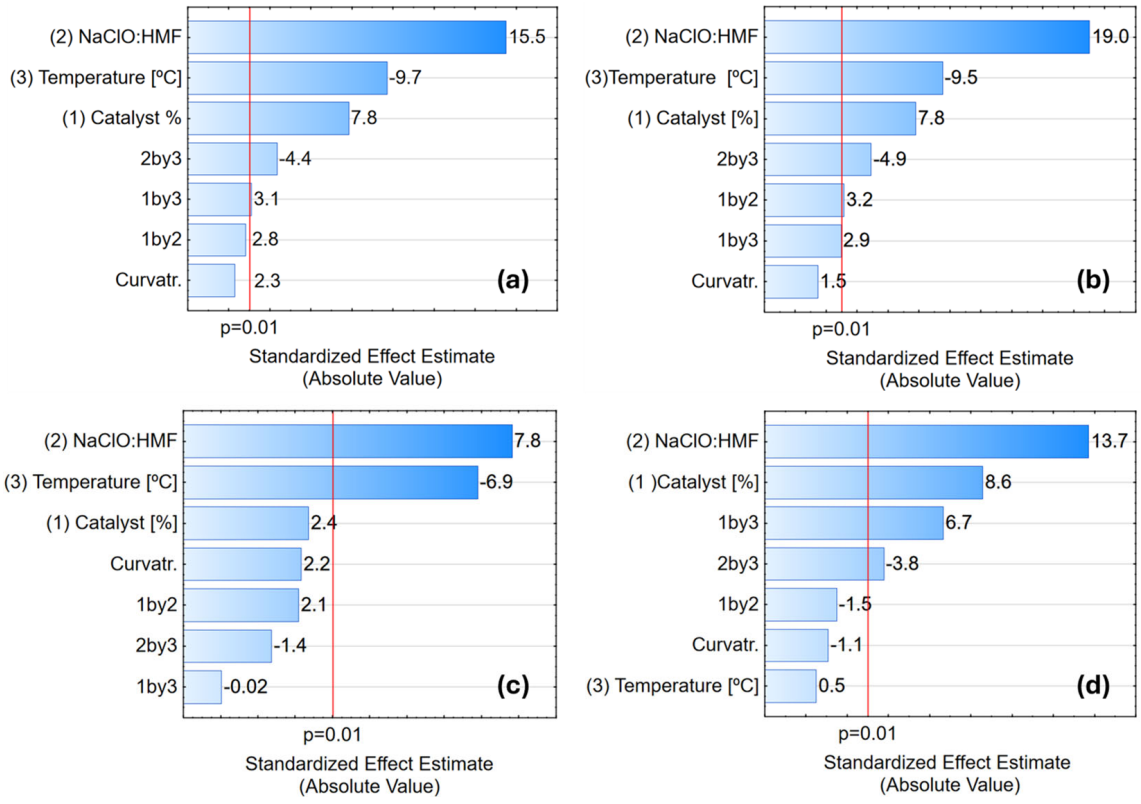


Figure 9. Pareto chart of the estimated effects of reaction variables on: (**a**) FDCA concentration; (**b**) FDCA yield; (**c**) FDCA selectivity; (**d**) HMF conversion.

In summary, the optimization study confirmed that both the concentration of active sites (via catalyst loading) and the availability of oxidant (via NaClO:HMF molar ratio) are critical for maximizing FDCA production. Mild reaction temperatures favored higher selectivity, likely due to the reduced formation of by-products and lower catalyst deactivation rates.

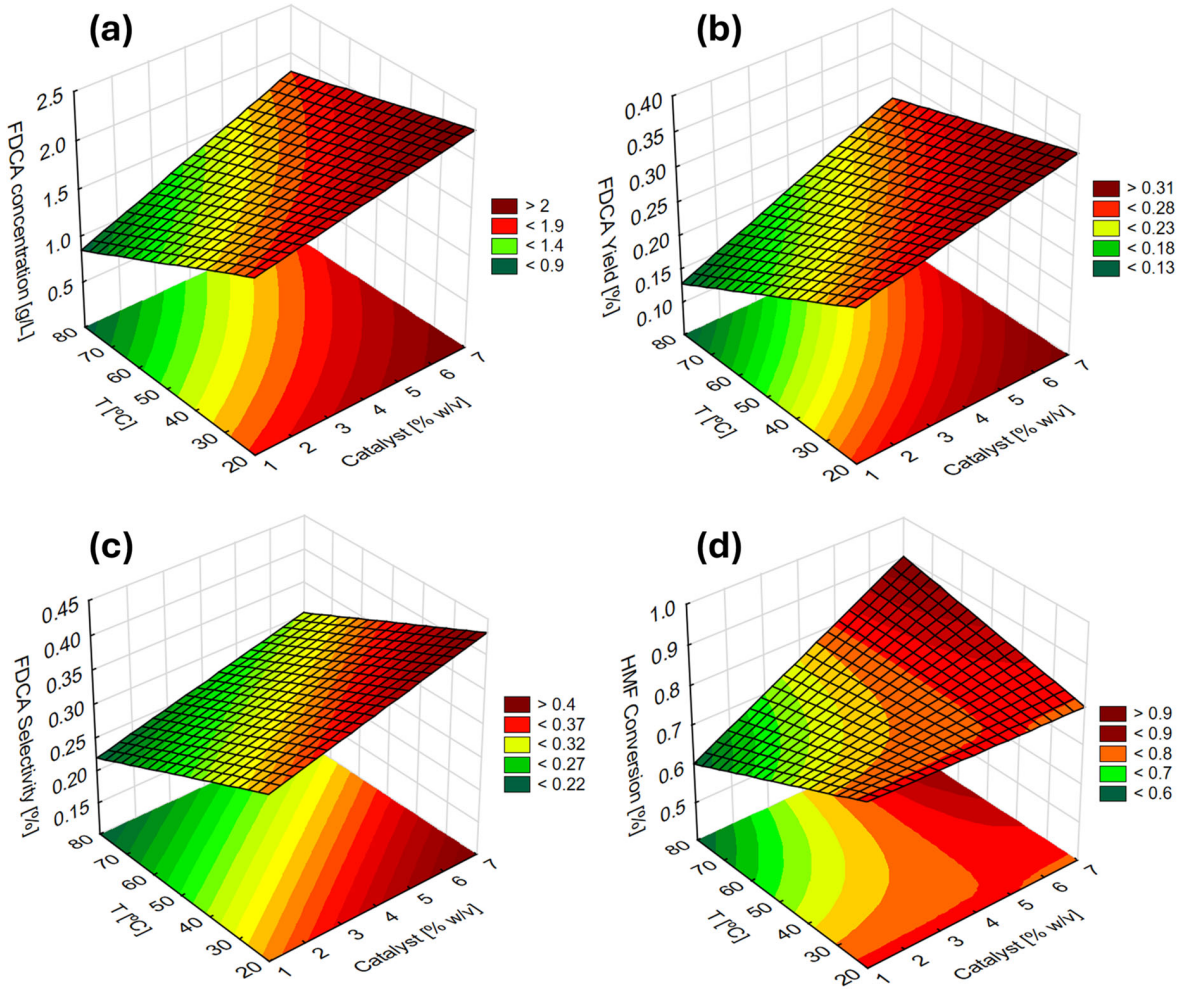


Figure 10. Response surface plot of the model responses for (**a**) FDCA concentration, (**b**) yield, (**c**) selectivity, and (**d**) HMF conversion as a function of catalyst loading and reaction temperature at a NaClO:HMF molar ratio of 12:1.

3.5. Reaction Kinetics Under Optimized Conditions

Once the optimal reaction parameters were identified, a new kinetic run was performed using the NiOx catalyst at 6% w/v, 25 °C, and a NaClO:HMF molar ratio of 12:1. As shown in Figure 11, FDCA yield increased 2.5 times, reaching 34.74% after 60 min, with an HMF conversion of 80.19%. Moreover, productivity increased markedly from an average of 0.02 g L^{-1} min^{-1} to 0.05 g L^{-1} min^{-1}, representing a 2.5-fold. This substantial improvement over the non-optimized condition underscores a significant performance gain that could contribute to the future economic viability of the process.

The reaction exhibited pseudo-first-order behavior with respect to HMF concentration, consistent with the assumption of excess oxidant and surface-mediated rate control. This finding is supported by Liu et al. [9], who also reported pseudo-first-order kinetics for HMF oxidation using Ni-based catalysts in the absence of added base. The observed activation under mild conditions reinforces the catalytic efficiency of NiOx and highlights the role of hydroxylated Ni(II)/Ni(III) sites in redox cycling.

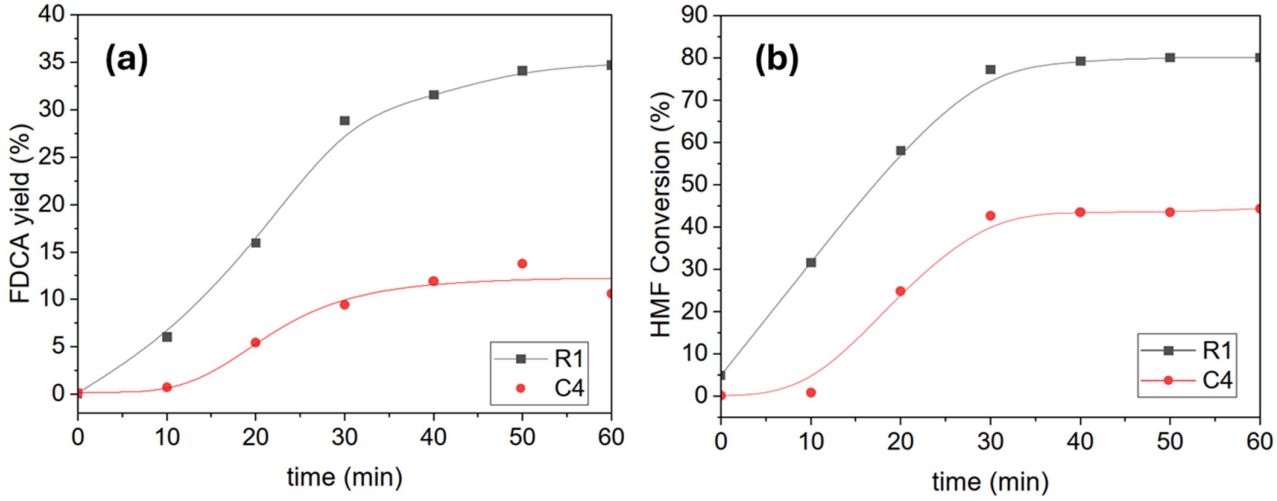


Figure 11. Kinetics of FDCA production from pure HMF using the NiOx catalyst: (**a**) FDCA yield; (**b**) HMF conversion. R1: kinetic study under the high-level conditions of the 2^3 factorial design, with a triplicate at the center point (6% *w*/*v* catalyst, T = 25 °C, and a NaClO:HMF molar ratio of 12:1); C4: conditions that gave the best result in the previous kinetic study (2% *w*/*v* catalyst, T = 25 °C, and a NaClO:HMF molar ratio of 6:1).

3.6. Catalyst Reusability and Stability

Catalyst recyclability is a critical parameter for industrial application. The NiOx catalyst was subjected to five consecutive oxidation cycles under optimized conditions. After each run, the catalyst was recovered by filtration, washed with deionized water, and dried before reuse.

As shown in Figure 12, FDCA yield remained stable across the cycles, with a slight decrease from 34.14% in the first cycle to 31.28% in the fifth cycle, indicating minimal catalyst deactivation.

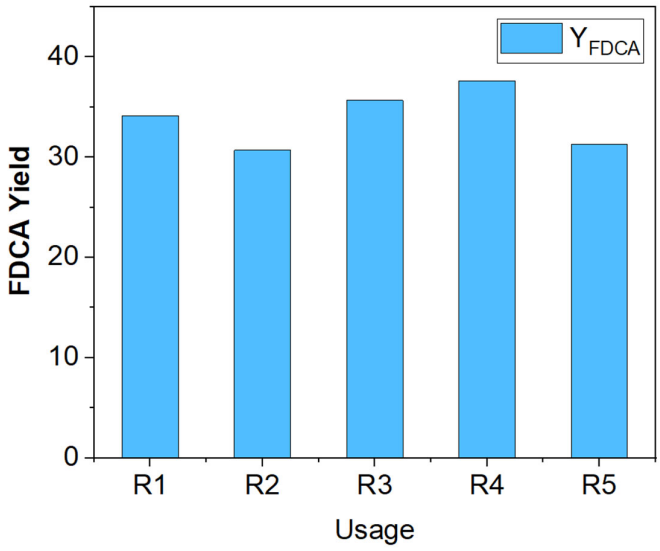


Figure 12. Performance of the NiOx catalyst (FDCA yield) over five successive reactions.

XRD analysis (Figure 13) of the spent catalyst confirmed the retention of the amorphous NiOx structure. No significant crystallization or peak shifts were observed, indicating structural stability. These observations are consistent with the absence of defined diffraction peaks such as those at 2θ ≈ 37.2°, 43.3°, and 62.9°, which had previously been assigned to the (1 1 1), (2 0 0), and (2 2 0) planes of NiO, in agreement with the face-centered cubic (fcc) structure (JCPDS card no. 47-1049), as discussed in Figure 3.

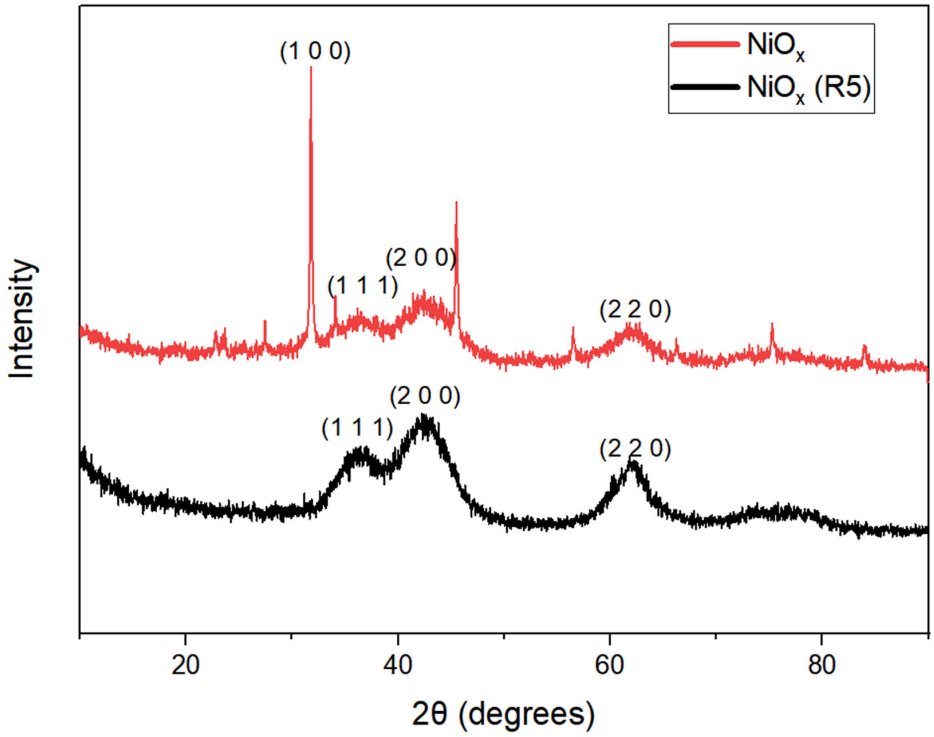


Figure 13. X-ray diffractograms of NiOx before and after five successive reactions.

This reinforces that the amorphous character of NiOx was preserved even after multiple catalytic cycles. The crystallite size was estimated to be 60 nm for NiOx after repeated use, using the Scherrer equation at the 43.3° peak.

SEM images (Figure 14a) showed preservation of surface morphology, with no evidence of sintering or severe agglomeration. The EDX spectrum (Figure 14b) confirmed the presence of the primary elements in the catalyst surface, nickel (Ni) and oxygen (O), with elemental compositions of 50.5% and 47.7%, respectively. The detection of minor elements such as chlorine (Cl) and sodium (Na) is attributed to residual impurities from the precursor reagents.

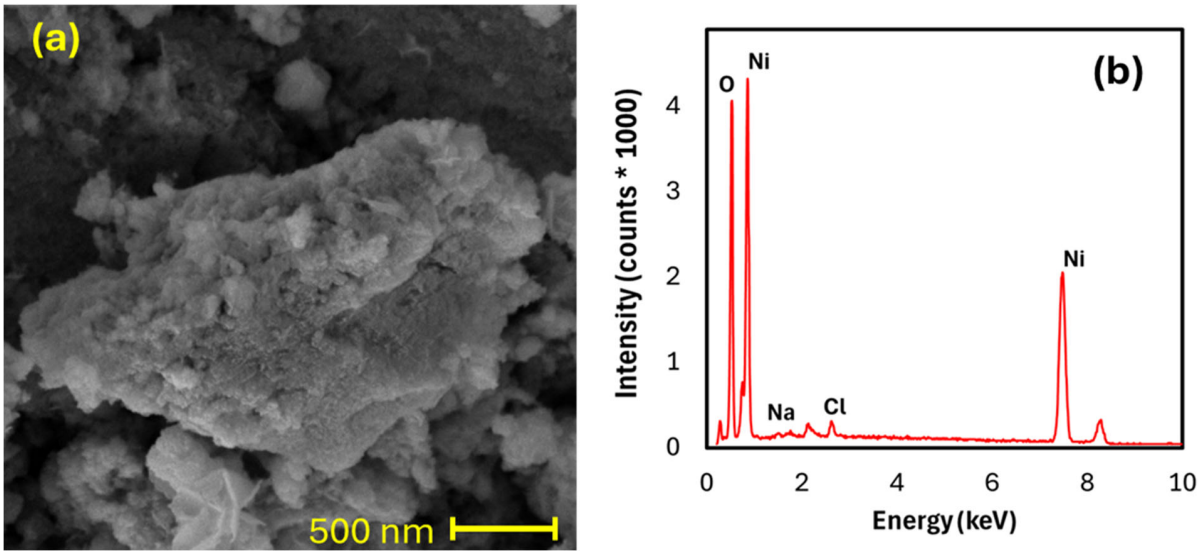


Figure 14. (**a**) SEM image of NiOx after five successive reactions at 100,000× magnification (500 nm scale bar). (**b**) EDX spectrum showing all the elements detected in the sample.

These results indicate that the NiOx catalyst exhibits excellent stability and resistance to oxidative degradation. This aligns with the findings of Holzhäuser et al. [15], who also reported stable performance of Ni-containing oxides over multiple cycles in HMF oxidation.

3.7. FDCA Production from Crude HMF

To assess the potential for FDCA production from crude HMF using NiOx as a catalyst, experiments were conducted using crude HMF obtained from the dehydration of glucose in water, using $NbOPO_4$ as catalyst. The resulting organic phase, enriched in HMF (~8.4 $g \cdot L^{-1}$), was directly submitted to oxidation without prior purification.

Under optimized reaction conditions, the NiOx catalyst yielded 5.43% FDCA, with 23.47% selectivity and 23.14% HMF conversion (Table 9). Although these values were lower than those obtained with pure HMF, they demonstrate the catalyst's tolerance to impurities and its potential for application in integrated biomass conversion schemes.

Table 9. Results of the reaction converting crude HMF to FDCA.

Results			
C_{FDCA} (gL^{-1})	Y_{FDCA} (%)	S_{FDCA} (%)	X_{HMF} (%)
0.39	5.43	23.47	23.14

This performance is notable, considering that crude HMF typically contains humins, organic acids, and sugar-derived by-products that can poison active sites. The ability of NiOx to remain active in such complex a matrix highlights its practical utility, especially in decentralized or biorefinery-type systems, where purification steps are minimized [16].

Compared to noble-metal-based systems, which require highly purified HMF [4,12], the NiOx catalyst shows performance under much milder and less controlled conditions, supporting its economic and environmental advantages.

Table 10 summarizes the catalytic performance of NiOx in comparison with literature data on base-free oxidation of crude HMF to FDCA. The table shows that FDCA yields were low in the non-optimized stage, where no purification steps were included. Although the performance of NiOx in this stage was modest, it presents distinct advantages, as follows: operates in water, without added base or organic solvents; mild reaction conditions (25 °C, atmospheric pressure); high stability and recyclability; tolerance to crude HMF.

These findings make NiOx an attractive candidate for low-cost, scalable FDCA production in green chemistry contexts. The process avoids the generation of saline waste typical of NaOH-neutralized routes and minimizes environmental impacts. Moreover, the catalyst synthesis is simple, relying on earth-abundant and low-toxicity materials.

These characteristics align with the current demands for sustainable chemicals, particularly in the context of biopolymer precursors like FDCA, whose market is expected to grow significantly with the development of PEF and other bio-based materials [32,33].

Furthermore, the NiOx catalyst demonstrated potential for the selective oxidation of HMF to FDCA under mild, base-free conditions. The material's structure–function relationships were elucidated through comprehensive characterization, and reaction optimization yielded results that are competitive with state-of-the-art systems. In addition, the catalyst's reusability supports its application in sustainable biorefinery platforms.

Table 10. Comparison of the experiments performed for FDCA production through selective oxidation of crude HMF.

Catalyst	HMF Origin	Solvent, Additive and/or Oxidant	Reaction Conditions	FDCA Yield (%)	References
% Pt/C	Fructose	Gama-valerolactone/H_2O (50:50)	110°C, PO_2 = 40 bar, 20 h, cat 7.5% (*w*/*v*), no HMF purification	0	[30]
Co-Mn	Cellulosic biomass	H_2O/$NaHCO_3$	120 °C, PO_2 = 10 bar, 5 h, cat 10% (*w*/*v*), non-optimized stage, no HMF purification	4.6	[31]
NiO_x	Glucose	H_2O and NaClO:HMF 12:1	25 °C, 50 min, cat 6% (*w*/*v*), non-optimized stage, no HMF purification	5.4	This study

4. Conclusions

This study demonstrated the viability of a nickel-based heterogeneous catalyst (NiOx) synthesized via a simple precipitation route without thermal treatment, for the selective oxidation of 5-hydroxymethylfurfural (HMF) into 2,5-furandicarboxylic acid (FDCA) under environmentally benign conditions. The catalyst exhibited a mesoporous structure, significant surface hydroxylation, and thermal stability up to 300 °C, all of which contributed to its catalytic performance in aqueous media, in the absence of added base. Among the four catalysts synthesized and evaluated, the amorphous NiOx material showed superior activity, achieving FDCA yields up to 34.14% and selectivity of 42.57% under optimized conditions (6% w/v catalyst, 25 °C, NaClO:HMF molar ratio of 12:1). Kinetic studies revealed that the controlled oxidant addition increased FDCA production by 2.28-fold. The strategy of feeding NaClO at a constant rate over 30 min led to both higher FDCA yield and greater HMF conversion. Reaction optimization using a 2^3 factorial design identified catalyst concentration and oxidant ratio as the most influential parameters. The option of a controlled oxidant dosing strategy enhanced product selectivity and reduced side reactions, confirming the importance of reaction engineering in maximizing yield. The NiOx catalyst exhibited excellent stability over five reuse cycles, with minimal loss of activity or structural integrity. Furthermore, it maintained catalytic performance in the oxidation of crude HMF obtained from glucose dehydration, highlighting its robustness and practical applicability in biorefinery settings. Compared to noble-metal-based systems, NiOx offers a low-cost, scalable, and sustainable alternative for FDCA production. Its ease of synthesis and effective operation under mild reaction conditions make it a promising candidate for industrial applications in the production of bio-based polymers, such as polyethylene furanoate (PEF). Future work should explore the mechanistic aspects of NiOx redox activity, the integration of this system into continuous flow reactors, and its application to a wider range of biomass-derived substrates. The findings reported here contribute meaningfully to the development of sustainable catalytic technologies for green chemical manufacturing.

Author Contributions: Conceptualization, J.P.A.S., S.I.M., and L.M.C.; Methodology, C.L.d.A.S., J.P.A.S., and L.M.C.; Software, C.L.d.A.S., J.P.A.S., and L.M.C.; Investigation, C.L.d.A.S., J.P.A.S., and L.M.C.; Resources, J.P.A.S., S.I.M., and L.M.C.; Writing—Original Draft, C.L.d.A.S. and L.M.C.; Writing—Review and Editing, C.L.d.A.S., S.I.M., and L.M.C.; Supervision, J.P.A.S., S.I.M., and L.M.C.; Project Administration, L.M.C.; Funding Acquisition, J.P.A.S. and L.M.C. All authors have read and agreed to the published version of the manuscript.

Funding: This research was funded by Fundação de Amparo à Pesquisa do Estado de São Paulo (FAPESP), project number 2017/24050-8, Brazil; Conselho Nacional de Desenvolvimento Científico

e Tecnológico (CNPq), Brazil; and Coordenação de Aperfeiçoamento de Pessoal de Nível Superior (CAPES), Brazil.

Data Availability Statement: The original contributions presented in this study are included in the article. Further inquiries can be directed to the corresponding author.

Acknowledgments: We thank Companhia Brasileira de Metalurgia e Mineração (CBMM) to donations the materials used for experiments.

Conflicts of Interest: The authors declare no conflicts of interest.

References

1. Lecona-Vargas, C.S.; Orsat, V.; Dumont, M.-J. Carbohydrate-Based Biorefineries for the Production of 5-Hydroxymethylfurfural and 2,5-Furandicarboxylic Acid and Their Separation and Purification Methods. *Biomass Convers. Biorefin* **2022**, *12*, 26575–26595. [CrossRef]
2. Dessbesell, L.; Souzanchi, S.; Venkateswara Rao, K.T.; Carrillo, A.A.; Bekker, D.; Hall, K.A.; Lawrence, K.M.; Tait, C.L.J.; Xu, C. Production of 2,5-Furandicarboxylic Acid (FDCA) from Starch, Glucose, or High-Fructose Corn Syrup: Techno-Economic Analysis. *Biofuels Bioprod. Biorefining* **2019**, *13*, 1234–1245. [CrossRef]
3. Gao, R.; Wang, J.; Liu, F.; Dai, H.; Zhang, X.; Wang, X.; Li, Y.; Zhu, J. Synthesis of Bio-Based Poly(Ester-Ether) Elastomers from 2,5-Furandicarboxylic Acid (FDCA) with Excellent Thermo-Mechanical Properties. *Polym. Degrad. Stab.* **2023**, *210*, 110292–110304. [CrossRef]
4. Hayashi, E.; Komanoya, T.; Kamata, K.; Hara, M. Heterogeneously-Catalyzed Aerobic Oxidation of 5-Hydroxymethylfurfural to 2,5-Furandicarboxylic Acid with MnO_2. *ChemSusChem* **2017**, *10*, 654–658. [CrossRef]
5. Jiang, M.; Hu, F.; Feng, G.; Zhang, H.; Hu, H.; Gan, T.; Huang, Z.; Zhang, Y. In-Situ Growth of MnO_2 on Hierarchical Porous Carbon Foam with Enhanced Oxygen Vacancy Concentration and Charge Transfer for Efficient Catalytic Oxidation of 5-Hydroxymethylfurfural. *Appl. Surf. Sci.* **2022**, *598*, 153849–153859. [CrossRef]
6. Gallo, J.M.R.; Alonso, D.M.; Mellmer, M.A.; Dumesic, J.A. Production and Upgrading of 5-Hydroxymethylfurfural Using Heterogeneous Catalysts and Biomass-Derived Solvents. *Green. Chem.* **2013**, *15*, 85–90. [CrossRef]
7. Biradar Tamboli, A.T.; Kirdant, S.P.; Jadhav, V.H. Metal-Free Approach towards Efficient Synthesis of FDCA Using a p-Toluene Sulfonic Acid (p-TSA)-Derived Heterogeneous Solid Acid Catalyst and Oxone over Two Steps from HMF, Fructose and Glucose. *New J. Chem.* **2022**, *46*, 10272–10279. [CrossRef]
8. Bonincontro, D.; Lolli, A.; Villa, A.; Prati, L.; Dimitratos, N.; Veith, G.M.; Chinchilla, L.E.; Botton, G.A.; Cavani, F.; Albonetti, S. AuPd-nNiO as an Effective Catalyst for the Base-Free Oxidation of HMF under Mild Reaction Conditions. *Green. Chem.* **2019**, *21*, 4090–4099. [CrossRef]
9. Liu, H.; Li, W.; Zuo, M.; Tang, X.; Zeng, X.; Sun, Y.; Lei, T.; Fang, H.; Li, T.; Lin, L. Facile and Efficient Two-Step Formation of a Renewable Monomer 2,5-Furandicarboxylic Acid from Carbohydrates over the NiOx Catalyst. *Ind. Eng. Chem. Res.* **2020**, *59*, 4895–4904. [CrossRef]
10. Zhang, W.; Li, Q.; Xia, H. Photocatalytic Oxidation of 5-Hydroxymethylfurfural to Furandicarboxylic Acid over the Au-Ag/TiO2 Catalysts under Visible Light Irradiation. *Appl. Surf. Sci.* **2023**, *613*, 156036–156047. [CrossRef]
11. Wang, S.; Feng, H.; Liu, T.; Deng, Y.; Zhang, M.; Zhao, S.; Han, J.; Zhang, X. Theoretical Exploration of the Origin of Alkaline Dependence in the Oxidation of 5-Hydroxymethylfurfural Catalyzed by NiO2Hx. *ACS Catal.* **2024**, *14*, 9860–9869. [CrossRef]
12. Zhu, Y.; Wei, J.; Wu, J.; Chen, R.; Tsiakaras, P.; Yin, S. Built-in Electric Field in NiO-CuO Heterostructures to Regulate the Hydroxide Adsorption Sites for 5-Hydroxymethylfurfural Electrooxidation Assisted Hydrogen Production. *J. Colloid. Interface Sci.* **2024**, *673*, 301–311. [CrossRef] [PubMed]
13. Luo, R.; Li, Y.; Xing, L.; Wang, N.; Zhong, R.; Qian, Z.; Du, C.; Yin, G.; Wang, Y.; Du, L. A Dynamic $Ni(OH)_2$-NiOOH/NiFeP Heterojunction Enabling High-Performance E-Upgrading of Hydroxymethylfurfural. *Appl. Catal. B* **2022**, *311*, 121357–121368. [CrossRef]
14. Herlina, I.; Krisnandi, Y.K.; Ridwan, M. Oxidation of 5-Hydroxymethylfurfural into 2,5-Furandicarboxylic Acid over CuO and NiO Modified Natural Sourced Hierarchical ZSM-5. *S. Afr. J. Chem. Eng.* **2024**, *47*, 75–82. [CrossRef]
15. Holzhäuser, F.J.; Janke, T.; Öztas, F.; Broicher, C.; Palkovits, R. Electrocatalytic Oxidation of 5-Hydroxymethylfurfural into the Monomer 2,5-Furandicarboxylic Acid Using Mesostructured Nickel Oxide. *Adv. Sustain. Syst.* **2020**, *4*, 1900151–1900156. [CrossRef]
16. Chen, Z.; Wang, Y.; Cheng, H.; Zhou, H. Integrated Chemo- and Biocatalytic Processes: A New Fashion toward Renewable Chemicals Production from Lignocellulosic Biomass. *J. Chem. Technol. Biotechnol.* **2023**, *98*, 331–345. [CrossRef]
17. Singh, D.; Batoo, K.M.; Hussain, S.; Kumar, A.; Aziz, Q.H.; Sheri, F.S.; Tariq, H.; Singh, P. Enhancement of the Photocatalytic Activity of RGO/NiO/Ag Nanocomposite for Degradation of Methylene Blue Dye. *RSC Adv.* **2024**, *14*, 2429–2438. [CrossRef]

18. Yang, Y.; Li, J.; Li, C.; Gong, M.; Wang, X.; Yang, X.; Wang, H.; Li, Y.-F.; Liu, Z.-P. The Identity of Nickel Peroxide as a Nickel Superoxyhydroxide for Enhanced Electrocatalysis. *JACS Au* **2023**, *3*, 2964–2972. [CrossRef]
19. Kumar, A.; Mustafa, M.A.; Fouly, A.; Bains, P.S.; Sharma, R.; Bisht, Y.S.; Awwad, E.M.; Singh, P. NiOx/PANI Nanocomposite Doped Carbon Paste as Electrode for Long-Term Stable and Highly Efficient Perovskite Solar Cells. *RSC Adv.* **2024**, *14*, 13374–13383. [CrossRef]
20. Gao, W.; Guan, X.; Wang, J.; Heinig, N.F.; Thomas, J.P.; Zhang, L.; Ding, K.; Leung, K.T. Supported NiOx Nanocatalysts on Graphene for Nonenzymatic Lactate Sensing. *ACS Appl. Nano Mater.* **2024**, *7*, 7162–7171. [CrossRef]
21. Zhang, H.; Gao, T.; Cao, Q.; Fang, W. Tailoring the Reactive Oxygen Species in Mesoporous NiO for Selectivity-Controlled Aerobic Oxidation of 5-Hydroxymethylfurfural on a Loaded Pt Catalyst. *ACS Sustain. Chem. Eng.* **2021**, *9*, 6056–6067. [CrossRef]
22. Christoskova, S.G.; Stoyanova, M.; Danova, N.; Argirov, O. Low-Temperature Methanol Oxidation on a Higher Nickel Oxide in Gaseous and Aqueous Phase. Part II. *Appl. Catal. A Gen.* **1998**, *173*, 101–105. [CrossRef]
23. He, H.; Yang, S.; Yu, K.; Ju, Y.; Sun, C.; Wang, L. Microwave Induced Catalytic Degradation of Crystal Violet in Nano-Nickel Dioxide Suspensions. *J. Hazard. Mater.* **2010**, *173*, 393–400. [CrossRef] [PubMed]
24. Ji, H.; Wang, T.; Zhang, M.; She, Y.; Wang, L. Simple Fabrication of Nano-Sized NiO2 Powder and Its Application to Oxidation Reactions. *Appl. Catal. A Gen.* **2005**, *282*, 25–30. [CrossRef]
25. Lai, T.-L.; Lee, C.-C.; Wu, K.-S.; Shu, Y.-Y.; Wang, C.-B. Microwave-Enhanced Catalytic Degradation of Phenol over Nickel Oxide. *Appl. Catal. B* **2006**, *68*, 147–153. [CrossRef]
26. Lai, T.-L.; Liu, J.-Y.; Yong, K.-F.; Shu, Y.-Y.; Wang, C.-B. Microwave-Enhanced Catalytic Degradation of 4-Chlorophenol over Nickel Oxides under Low Temperature. *J. Hazard. Mater.* **2008**, *157*, 496–502. [CrossRef] [PubMed]
27. Zhang, H.; Fan, B.; Bian, L.; Tang, Q.; Cao, Q.; Fang, W. Influence of NiO-Calcination on Pt-Supported Catalyst for Selective Oxidation of 5-Hydroxymethylfurfural. *Catal. Commun.* **2023**, *184*, 106791–106798. [CrossRef]
28. Rathod, P.V.; Jadhav, V.H. Efficient Method for Synthesis of 2,5-Furandicarboxylic Acid from 5-Hydroxymethylfurfural and Fructose Using Pd/CC Catalyst under Aqueous Conditions. *ACS Sustain. Chem. Eng.* **2018**, *6*, 5766–5771. [CrossRef]
29. Vuyyuru, K.R.; Strasser, P. Oxidation of Biomass Derived 5-Hydroxymethylfurfural Using Heterogeneous and Electrochemical Catalysis. *Catal. Today* **2012**, *195*, 144–154. [CrossRef]
30. Motagamwala, A.H.; Won, W.; Sener, C.; Alonso, D.M.; Maravelias, C.T.; Dumesic, J.A. Toward Biomass-Derived Renewable Plastics: Production of 2,5-Furandicarboxylic Acid from Fructose. *Sci. Adv.* **2018**, *4*, 9722–9729. [CrossRef]
31. Rao, K.T.V.; Rogers, J.L.; Souzanchi, S.; Dessbesell, L.; Ray, M.B.; Xu, C.C. Inexpensive but Highly Efficient Co–Mn Mixed-Oxide Catalysts for Selective Oxidation of 5-Hydroxymethylfurfural to 2,5-Furandicarboxylic Acid. *ChemSusChem* **2018**, *11*, 3323–3334. [CrossRef]
32. Reports and Data 2,5-Furandicarboxylic Acid (FDCA) Market. Available online: https://www.reportsanddata.com/report-detail/2-5-furandicarboxylic-acid-fdca-market (accessed on 7 April 2023).
33. KBV Research POLYETHYLENE Terephthalate Market Size, Share & Industry Forecast Report. Available online: https://www.kbvresearch.com/polyethylene-terephthalate-market (accessed on 27 September 2024).

Disclaimer/Publisher's Note: The statements, opinions and data contained in all publications are solely those of the individual author(s) and contributor(s) and not of MDPI and/or the editor(s). MDPI and/or the editor(s) disclaim responsibility for any injury to people or property resulting from any ideas, methods, instructions or products referred to in the content.